Brittle Fracture Due to an Array of Microcracks

N. A. Fleck

Proceedings: Mathematical and Physical Sciences, Vol. 432, No. 1884 (Jan. 8, 1991), 55-76.

Stable URL:
http://links.jstor.org/sici?sici=0962-8444%2819910108%29432%3A1884%3C55%3ABFDTAA%3E2.0.CO%3B2-9

Proceedings: Mathematical and Physical Sciences is currently published by The Royal Society.

Brittle fracture due to an array of microcracks

By N. A. Fleck

Department of Engineering, Cambridge University, Cambridge CB2 1PZ, U.K.

The method of distributed dislocations is used to analyse the response of an infinite elastic solid containing a single periodic array of inclined curved cracks. Uniform remote loading is applied to the body, and the cracks are of arbitrary but identical shapes. Expressions are derived for the stress intensity factors at each crack tip, the crack displacement profile and the extra compliance of the body due to the presence of the cracks. For an array of straight cracks, the stress intensity factors, and the extra compliance are found as a function of crack orientation and spacing.

Using this framework, we examine brittle fracture by the development of a periodic array of cracks in a solid which suffers all combinations of remote proportional loading. The solution for remote shear is explored in detail. The various types of response are summarized in a fracture map, and are compared with experimental observations for polymers and rocks.

1. Introduction

When an elastic body containing a random distribution of flaws is subjected to remote shear, failure may occur by the growth and coalescence of tensile microcracks in a band. This failure mechanism is known to occur in the case of the amorphous thermoplastics polycarbonate and polymethyl methacrylate (Fleck & Wright 1989) and in rocks (see, for example, Ramsay 1967; Pollard *et al.* 1982), where the cracks are referred to as echelon cracks. The typical morphology of the microcracks is shown in figure 1. Failure under remote shear due to tensile microcracking also occurs in fibrous composites with polymeric or ceramic matrices (Purslow 1981; Evans 1985). When a fibre is pulled out from the composite, or when two layers delaminate, the matrix can suffer shear failure by this cracking process (see figure 1).

This failure process of shear localization is similar in qualitative terms to shear localization phenomena in metals where the matrix material is plastic (Yamamoto 1978; Anderson *et al.* 1989; Fleck *et al.* 1989), or is viscous (Fleck 1988). Failure is due to the nucleation, growth and coalescence of voids or cracks in a localized band, with material outside the band behaving essentially in a rigid manner.

In this paper, we calculate the evolution of a periodic array of cracks under remote proportional loading. Straight cracks are assumed to nucleate to a length $2a_0$ which is much smaller than the crack spacing $2b$. The initial orientation of the cracks is taken to be normal to the direction of maximum principal tensile stress. We assume each crack of the periodic array grows into a curved shape without kinking, under the condition that the local mode II stress intensity factor K_{II} at the crack tip vanishes. This has been substantiated by many experiments (see, for example, Erdogan & Sih 1963). The solution method adopted is that of solving a singular integral equation for a distribution of dislocations, using a similar technique to that developed by Erdogan & Gupta (1972).

The outline of the paper is as follows. The governing integral equation is

Proc. R. Soc. Lond. A (1991) **432**, 55–76
Printed in Great Britain

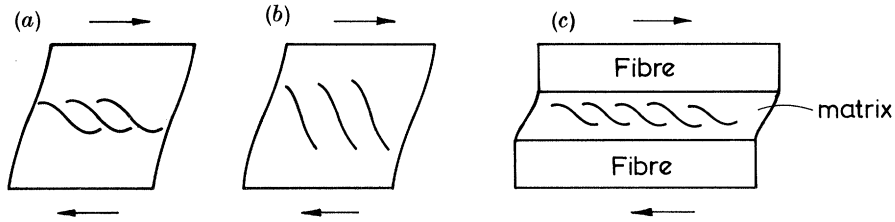

Figure 1. Typical morphology of an array of microcracks in a brittle solid, under predominantly remote shear. (*a*) Amorphous polymers, (*b*) isotropic rocks, and (*c*) fibre composites.

formulated, and the numerical solution procedure is outlined. Some results for an array of inclined straight cracks are given and the issue of crack stability for a strip of finite height under fixed remote displacements is addressed. The evolution of crack shape for the case of remote simple shear is given in some detail, and compared with the case of an array of collinear cracks under remote tension, as found by Koiter (1959). Finally, the evolution of crack shape is described for a variety of remote loadings, and a fracture map is constructed. This fracture map summarizes the cracking pattern as a function of remote loading; it is used in two case studies to predict the nature of the remote loading from observation of the shape of the fracture surfaces.

2. Formulation of the integral equation

We may solve the problem of a periodic array of curved cracks under remote stress σ_{ij}^{∞} by the method of superposition of dislocations. Let $b_x(\xi)$ and $b_y(\xi)$ be the x and y components of an edge dislocation arranged in a periodic array in the complex plane, $z = x+\mathrm{i}y$. The dislocations are located as shown in figure 2 at z_0+2nb where $z_0 = x_0+\mathrm{i}y_0$ is the location of the dislocation adjacent to the origin, $2b$ is the dislocation spacing, and n is an integer taking all values. We assume the material is isotropic and linearly elastic, with a shear modulus μ and Poisson ratio ν. The stresses σ_{ij} and displacements u_i induced by the dislocation can be obtained by Muskhelishvili methods and are given for plane strain conditions as,

$$\left.\begin{aligned} \sigma_x+\sigma_y &= 2(\phi'(z)+\overline{\phi'(z)}),\\ \sigma_y-\sigma_x+\mathrm{i}2\sigma_{xy} &= 2[(\bar{z}-z)\,\phi''(z)+\Omega'(z)-\phi'(z)],\\ 2\mu(u_x+\mathrm{i}u_y) &= (3-4\nu)\,\phi(z)+(\bar{z}-z)\,\overline{\phi'(z)}-\overline{\Omega(z)}, \end{aligned}\right\} \tag{2.1}$$

where the Muskhelishvili potentials $\phi(z)$ and $\Omega(z)$ are expressed in terms of $A(z_0) \equiv \mu(b_y-\mathrm{i}b_x)/4\pi(1-\nu)$ as,

$$\begin{aligned} \phi(z) &= A\ln\sin\left((\pi/2b)\,(z-z_0)\right),\\ \Omega(z) &= \bar{A}\ln\sin\left((\pi/2b)\,(z-z_0)\right)-A(\pi/2b)\,(\bar{z}_0-z_0))\cot\left((\pi/2b)\,(z-z_0)\right). \end{aligned} \tag{2.2}$$

These potentials give the required periodicity in stresses, and the desired multi-valuedness in displacements on prescribing a Burgers circuit around any of the dislocations. Near the dislocations the stresses vary as $(z-z_0)^{-1}$, and at large $|y|$ stresses decay as z^{-1}, as required.

Now consider the dislocations located on a periodic array of curves of spacing $2b$, with a single dislocation on each curve. Each curve defines the shape of a crack. We shall consider the problem of a distribution of dislocations on each curve such that the traction on each curve is equal and opposite to that given by the remote homogeneous stress field. Then, the curves become traction free and are equivalent mathematically to cracks.

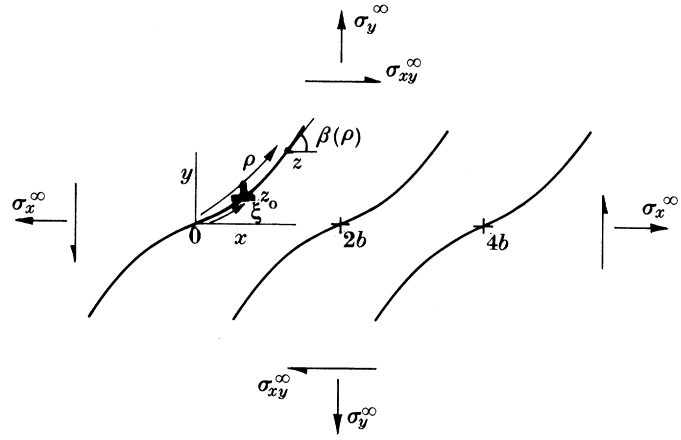

Figure 2. Crack geometry.

Define the shape of the curve shown in figure 2 in terms of distance ρ from the origin. We assume that the inclination β of the curve is known as a function of ρ; this defines the shape of the curve. Writing (t, n) as the tangential and normal directions to the curve, the stress components at a point ρ on the curve due to a dislocation at a point ξ is derived from (2.1) and (2.2) as,

$$\sigma_n(\rho)+\mathrm{i}\sigma_{nt}(\rho) = A(\xi)\,H_1(z_0, z)+\bar{A}(\xi)\,H_2(z_0, z), \tag{2.3}$$

where

$$H_1(z_0, z) = (\pi/2b)\cot((\pi/2b)(z-z_0))(1-\mathrm{e}^{\mathrm{i}2\beta(\rho)})+(\pi/2b)^2\,\mathrm{e}^{\mathrm{i}2\beta(\rho)}\left[\frac{(z-z_0)-(\bar{z}-\bar{z}_0)}{\sin^2((\pi/2b)(z-z_0))}\right]$$

and $$H_2(z_0, z) = (\pi/2b)\cot((\pi/2b)(\bar{z}-\bar{z}_0))+(\pi/2b)\,\mathrm{e}^{\mathrm{i}2\beta(\rho)}\cot((\pi/2b)(z-z_0)).$$

The array of cracks is represented by a distribution of dislocations laying along each curve such that the net traction vanishes on each curve. That is, the distribution of dislocation $A(\xi)$ must satisfy the condition along the curve C,

$$p_n(\rho)+\mathrm{i}p_{nt}(\rho)+\int_C A(\xi)\,H_1(z_0, z)+\bar{A}(\xi)\,H_2(z_0, z)\,\mathrm{d}\xi = 0. \tag{2.4}$$

Here, p_n and p_{nt} are the normal and shear stresses due to the remote loading σ_{ij}^∞; they are given by

$$p_n+\mathrm{i}p_{nt} = \tfrac{1}{2}(\sigma_y^\infty-\sigma_x^\infty+\mathrm{i}2\sigma_{xy}^\infty)\,\mathrm{e}^{\mathrm{i}2\beta(\rho)}+\tfrac{1}{2}(\sigma_x^\infty+\sigma_y^\infty). \tag{2.5}$$

To proceed, we express z and z_0 in terms of ρ and ξ respectively. After separating out the Cauchy integral, (2.4) may be rewritten as

$$p_n(\rho)+\mathrm{i}p_{nt}(\rho) = \int_{-a}^{a} 2\mathrm{e}^{\mathrm{i}\beta(\rho)}\bar{A}(\xi)\frac{\mathrm{d}\xi}{\xi-\rho}+\int_{-a}^{a} A(\xi)\,K(z_0, z)+\bar{A}(\xi)\,L(z_0, z)\,\mathrm{d}\xi \quad (|\rho|<a), \tag{2.6}$$

where

$$K(z_0, z) = (\pi/2b)(1-\mathrm{e}^{\mathrm{i}2\beta(\rho)})\cot((\pi/2b)(z_0-z))+(\pi/2b)^2\,\mathrm{e}^{\mathrm{i}2\beta(\rho)}\left[\frac{(z_0-z)-(\bar{z}_0-\bar{z})}{\sin^2((\pi/2b)(z_0-z))}\right]$$

and

$$L(z_0, z) = (\pi/2b)\cot((\pi/2b)(\bar{z}_0-\bar{z}))+(\pi/2b)\,\mathrm{e}^{\mathrm{i}2\beta(\rho)}\cot((\pi/2b)(z_0-z))-2\mathrm{e}^{\mathrm{i}\beta(\rho)}/(\xi-\rho).$$

The first integral in (2.6) is the Cauchy principal value integral, and K, L contain removable singularities at $\xi = \rho$. For the case of straight cracks at an inclination β to the x axis, equation (2.6) can be simplified to,

$$p_n + \mathrm{i}p_{nt} = 2\mathrm{e}^{\mathrm{i}\beta} \int_{-a}^{a} \bar{A}(\xi) \frac{\mathrm{d}\xi}{\xi - \rho} + \int_{-a}^{a} A(\xi) K(\xi, \rho) + \bar{A}(\xi) L(\xi, \rho)\, \mathrm{d}\xi \quad (|\rho| < a), \quad (2.7)$$

where

$$K(\xi, \rho) = (\pi/2b)(1 - \mathrm{e}^{\mathrm{i}2\beta}) \cot((\pi/2b)\mathrm{e}^{\mathrm{i}\beta}(\xi - \rho)) + \mathrm{e}^{\mathrm{i}2\beta}(\mathrm{e}^{\mathrm{i}\beta} - \mathrm{e}^{-\mathrm{i}\beta})(\pi/2b)^2 \frac{\xi - \rho}{\sin^2((\pi/2b)\mathrm{e}^{\mathrm{i}\beta}(\xi - \rho))},$$

$$L(\xi, \rho) = (\pi/2b)[\cot((\pi/2b)\mathrm{e}^{-\mathrm{i}\beta}(\xi - \rho)) + \mathrm{e}^{\mathrm{i}2\beta} \cot((\pi/2b)\mathrm{e}^{\mathrm{i}\beta}(\xi - \rho)) - 4b\,\mathrm{e}^{\mathrm{i}\beta}/\pi(\xi - \rho)]$$

and

$$p_n + \mathrm{i}p_{nt} = \tfrac{1}{2}(\sigma_y^\infty - \sigma_x^\infty + \mathrm{i}2\sigma_{xy}^\infty)\mathrm{e}^{\mathrm{i}2\beta} + \tfrac{1}{2}(\sigma_x^\infty + \sigma_y^\infty).$$

3. Solution of the integral equation

A procedure similar to that outlined by Erdogan & Gupta (1972) is used to solve the integral equation (2.6) and (2.7). Consider first the case of curved cracks.

With the change of variables $\xi = at$, the distribution $A(\xi)$ is taken to be

$$A(\xi) \equiv \frac{\mathrm{e}^{\mathrm{i}\beta(\xi)}}{(1 - t^2)^{\frac{1}{2}}} \sum_{j=0}^{N-1} c_j T_j(t), \quad \xi = at, \quad (3.1)$$

where $T_j(t)$ is the Chebyshev polynomial of the first kind of degree j and the cs are complex coefficients which must be determined by the solution process. The number of terms N is chosen to be sufficiently large to give an accuracy of 0.1% (typically, $N = 40$). The symmetry of the problem dictates that the cracks of length $2a$ possess point symmetry about their centres. Thus $A(\xi)$ is an odd function. For reasons of optimizing the numerical implementation of the method we use a complete representation for $A(\xi)$ and include the even terms. An alternative formulation of the integral equation assumes explicitly that the even coefficients vanish; such a formulation does not provide for much economy in computational time or for much gain in accuracy, as discussed by Erdogan & Gupta (1972). The alternative formulation was therefore not used in the present study.

When substituted into (2.6) the representation for A leads to an equation of the form

$$p_n(\rho_r) + \mathrm{i}p_{nt}(\rho_r) = \sum_{j=1}^{N-1} I_1(r, j)\, \bar{c}_j + \sum_{j=0}^{N-1} I_2(r, j)\, c_j + \sum_{j=0}^{N-1} I_3(r, j)\, \bar{c}_j, \quad (r = 1, \ldots, N-1), \quad (3.2)$$

where the terms I_1 to I_3 are

$$\left.\begin{aligned} I_1(r, j) &= \frac{2\pi}{N} \sum_{k=1}^{N} \frac{\exp(\mathrm{i}(\beta(\rho_r) - \beta(\xi_k)))}{t_k - u_r} T_j(t_k), \\ I_2(r, j) &= \frac{\pi a}{N} \sum_{k=1}^{N} \mathrm{e}^{\mathrm{i}\beta(\xi_k)} T_j(t_k) K(z_0(\xi_k), z(\rho_r)), \\ I_3(r, j) &= \frac{\pi a}{N} \sum_{k=1}^{N} \mathrm{e}^{-\mathrm{i}\beta(\xi_k)} T_j(t_k) L(z_0(\xi_k), z(\rho_r)), \end{aligned}\right\} \quad (3.3)$$

$$\xi_k = at_k, \quad \rho_r = au_r \quad t_k = \cos((\pi/2N)(2k - 1)), \quad u_r = \cos(\pi r/N).$$

Equations (3.2) and (3.3) follow directly from (2.6) by using the numerical integration scheme of Erdogan & Gupta (1972). The main formulas are

$$\left.\begin{aligned} &\int_{-1}^{1} \frac{f(t)}{t-u_r} \frac{\mathrm{d}t}{(1-t^2)^{\frac{1}{2}}} \approx \frac{\pi}{N} \sum_{k=1}^{N} \frac{f(t_k)}{t_k-u_r}, \\ &t_k = \cos(\pi/2N)(2k-1), \quad u_r = \cos(\pi r/N) \quad (r = 1, \ldots, N-1) \end{aligned}\right\} \tag{3.4}$$

and the Gauss–Chebyshev integration formula

$$\int_{-1}^{1} \frac{f(t)}{(1-t^2)^{\frac{1}{2}}} \mathrm{d}t \approx \frac{\pi}{N} \sum_{k=1}^{N} f(t_k), \quad T_N(t_k) = 0, \tag{3.5}$$

where $f(t)$ is analytic in $|t| \leqslant 1$.

In addition to equation (3.2) is the closure condition that the cracks produce no net slip in the solid, or

$$\int_{-a}^{a} A(\xi)\, \mathrm{d}\xi = 0. \tag{3.6}$$

The integral may be evaluated using the Gauss–Chebyshev formula to give

$$\sum_{j=0}^{N-1} \sum_{k=1}^{N} \mathrm{e}^{\mathrm{i}\beta(\xi_k)} T_j(t_k)\, c_j = 0, \quad t_k = \cos((\pi/2N)(2k-1)), \quad k = 1, \ldots, N. \tag{3.7}$$

We have now reduced the integral equation (2.6) to a linear system of $2N-2$ equations from (3.2), and 2 equation from (3.7) in $2N$ unknowns for $\mathrm{Re}\{c_j\}$ and $\mathrm{Im}\{c_j\}$. This set of $2N$ unknowns is used to satisfy the left-hand side of (3.2) at the $N-1$ collocation points $\rho_r = au_r$ $(r = 1, \ldots, N-1)$.

3.1. *Crack advance algorithm*

We calculate the continuous evolution of the crack profile under remote proportional loading. Each crack advances with no kinking, under the condition that K_{II} vanishes at the crack tip.

The crack is assumed to advance in steps Δa, with the curvature κ constant over each increment Δa. Thus the crack is represented by a curve of piecewise constant curvature. This representation gives simple expressions for $\beta(\rho)$ and $z(\rho)$; for a segment of the curve starting at ρ_{i} we have

$$\beta(\rho) = \beta_{\mathrm{i}} + \kappa_{\mathrm{i}}(\rho - \rho_{\mathrm{i}}), z(\rho) = z_{\mathrm{i}} - (\mathrm{i}/\kappa_{\mathrm{i}})(\mathrm{e}^{\mathrm{i}\beta(\rho)} - \mathrm{e}^{\mathrm{i}\beta_{\mathrm{i}}}), \tag{3.8}$$

where the subscript i refers to the value at the beginning of the segment.

The solution procedure is as follows. We consider an initial straight crack of short length $a/b = 0.1$, where $2a$ is the crack length and $2b$ is the crack spacing. The angle of the initial crack β_0 is chosen to be normal to the direction of maximum principal tensile stress. Since the cracks are small initially, they interact only very weakly and suffer similar loading to that of an isolated crack.

The cracks are advanced in steps $\Delta a/b = 0.2$ typically, such that K_{II} vanishes at the new crack tip. For each crack advance step, a Newton–Raphson scheme is used to search out a value for κ such that $K_{\mathrm{II}}/K_{\mathrm{I}}$ vanishes at the new crack tip. With crack advance, the cracks interact to an increasing degree and the number of equations $2N$ must be increased. Typically, $2N = 160$ when the cracks approach to within $0.1b$ of

each other and the calculation is stopped. As expected from symmetry, $A(\xi)$ is calculated to be an odd function: the even coefficients c_0, c_2, c_4, ..., vanish. Calculations were performed on a VAX workstation and required approximately 10 h of CPU time for growth of the cracks to coalescence.

3.2. *Calculation of stress intensity factors, crack opening and the extra compliance*

A direct calculation shows that the stress intensity factors are given by

$$K_{\mathrm{I}}+\mathrm{i}K_{\mathrm{II}} = (2\pi)^{\frac{3}{2}} \lim_{\epsilon \to 0^-} (-\epsilon)^{\frac{1}{2}} \mathrm{e}^{\mathrm{i}\beta(a)} \bar{A}(a+\epsilon),$$

which, with (3.1), reduces to

$$K_{\mathrm{I}}+\mathrm{i}K_{\mathrm{II}} = 2\pi^{\frac{3}{2}} a^{\frac{1}{2}} \sum_{j=0}^{N-1} \bar{c}_j. \tag{3.9}$$

Thus, the stress intensity factors are known directly from the solution for $\{c_j\}$.

The crack opening displacement is defined as the jump in displacement normal to each crack $\tilde{u}_n$ and transverse to each crack $\tilde{u}_t$. This displacement profile is calculated by integration of the dislocation density,

$$\tilde{u}_t(\rho)+\mathrm{i}\tilde{u}_n(\rho) = \mathrm{e}^{-\mathrm{i}\beta(\rho)} \int_{\rho}^{a} b_x(\xi)+\mathrm{i}b_y(\xi)\,\mathrm{d}\xi. \tag{3.10}$$

Using the relation between dislocation density $A(\xi)$ and the Burgers vector $A(\xi) \equiv \mu(b_y-\mathrm{i}b_x)/4\pi(1-\nu)$, and using the representation for $A(\xi)$ (equation (3.1)), equation (3.10) becomes

$$\tilde{u}_t(\rho)+\mathrm{i}\tilde{u}_n(\rho) = \frac{\mathrm{i}4\pi(1-\nu)}{\mu} \mathrm{e}^{-\mathrm{i}\beta(\rho)}\, a \int_{\rho/a}^{1} \frac{\mathrm{e}^{\mathrm{i}\beta(t)}}{(1-t^2)^{\frac{1}{2}}} \sum_{j=0}^{N-1} c_j T_j(t)\,\mathrm{d}t. \tag{3.11}$$

The integral on the right-hand side is evaluated numerically using a Gauss–Kronrod rule.

We now introduce the notion of an additional compliance due to the array of cracks. Under remote loading σ_y^∞, σ_{xy}^∞ the presence of the cracks gives rise to an additional displacement $\Delta u_x, \Delta u_y$ between remote material above the crack band and remote material below the cracked band. Let $\boldsymbol{N}$ be the unit normal to the crack array, such that $\boldsymbol{N}$ is aligned with the y direction of figure 2. Since the solid is linear we can define an extra compliance C_{ij} which relates Δu_i to the remote traction $\sigma_{ij}^\infty N_j$ by

$$\Delta u_i E/2b(1-\nu^2) = C_{ij}\,\sigma_{jk}^\infty N_k. \tag{3.12}$$

The extra compliance is a real, symmetric positive-definite tensor. Its components may be calculated from the following expression which is proved in the Appendix.

$$2b(\sigma_y^\infty \Delta u_y + \sigma_{xy}^\infty \Delta u_x) = \int_{-a}^{a} n_y \sigma_{xy}^\infty \tilde{u}_x + (n_x \sigma_{xy}^\infty + n_y \sigma_y^\infty)\,\tilde{u}_y\,\mathrm{d}\xi \tag{3.13}$$

where $\boldsymbol{n}(\xi)$ is the unit normal to the cracks and $\tilde{u}_x(\xi), \tilde{u}_y(\xi)$ are the crack opening displacements in the x and y directions respectively. The components C_{11}, C_{22}, $C_{12} = C_{12}$ are obtained by considering three loading cases: (i) $\sigma_y^\infty = 1$, other $\sigma_{ij}^\infty = 0$; (ii) $\sigma_{xy}^\infty = 1$, other $\sigma_{ij}^\infty = 0$; and (iii) $\sigma_y^\infty = \sigma_{xy}^\infty = 1$, other $\sigma_{ij}^\infty = 0$. These loading cases are used to solve the system of equations (3.12) in the unknowns C_{ij}.

The integrals on the right-hand side of (3.13) were evaluated using the Gauss–Chebyshev integration rule after some manipulation.

3.3. *Case of straight cracks*

The analysis of an array of straight cracks is somewhat simpler than that for curved cracks, and the integral equation (3.2) reduces to

$$p_n + \mathrm{i}p_{nt} = \sum_{j=1}^{N-1} J_1(r,j)\,\bar{c}_j + \sum_{j=0}^{N-1} J_2(r,j)\,c_j + \sum_{j=0}^{N-1} J_3(r,j)\,\bar{c}_j \quad (r = 1,\ldots,N-1), \tag{3.14}$$

where
$$J_1(r,j) = \frac{2\pi}{N}\sum_{k=1}^{N}\frac{T_j(t_k)}{t_k - u_r},\; J_2(r,j) = \frac{\pi a}{N}\mathrm{e}^{\mathrm{i}\beta}\sum_{k=1}^{N} T_j(t_k)\,K(at_k, au_r),$$

$$J_3(r,j) = \frac{\pi a}{N}\mathrm{e}^{-\mathrm{i}\beta}\sum_{k-1}^{N} T_j(t_k)\,L(at_k, au_r),\; u_r = \cos(\pi r/N),\; t_k = \cos((\pi/2N)(2k-1)).$$

The Fredholm kernels K, L for the straight crack are given by equation (2.7).

Since the distribution dislocation for each crack does not produce a net slip in the solid, equation (3.6) applies. On substitution of the representation (3.1) for $A(\xi)$, the integral in (3.6) may be evaluated for an array of straight cracks to give

$$c_0 = 0. \tag{3.15}$$

The $N-1$ equations (3.14), plus equation (3.15) are solved by gaussian elimination; the stress intensity factors and crack opening profile are calculated using (3.9) and (3.11), as before. We can perform the integrals for the extra displacement in closed form, and equation (3.13) becomes

$$2b(\sigma_y^\infty\,\Delta u_y + \sigma_{xy}^\infty\,\Delta u_x) = n_y\,\sigma_{xy}^\infty\,d_1 + (n_x\,\sigma_{xy}^\infty + n_y\,\sigma_y^\infty)\,d_2, \tag{3.16}$$

where
$$d_1 + \mathrm{i}d_2 \equiv (\mathrm{i}2(1-\nu)\,\pi^2 a^2/\mu)\,\mathrm{e}^{\mathrm{i}\beta}\,c_1.$$

Finally, the extra compliance C_{ij} is calculated in a similar manner to that described for the curved cracks.

4. Some results for straight cracks

In this section we shall examine the degree to which an array of straight cracks shield each other. Consider a cracked band subjected to remote tension, σ_y^∞. For cracks with a normal vector at a small angle to the direction of remote uniaxial tension we shall show that there exists a range of crack spacings over which the cracks repel each other. When the cracks are closer together or farther apart they attract each other.

The stress intensities and extra compliance are then given as a function of crack spacing and crack orientation.

4.1. *Crack–crack repulsion*

Consider an array of straight cracks at orientation $\beta = -5°$ under remote tensile loading $\sigma_y^\infty = \sigma$, as shown in figure 3. When the cracks are widely spaced the mode II stress intensity factor K_{II} is negative and the cracks attract each other: with crack advance branch cracks will form towards the neighbouring crack tip. The same

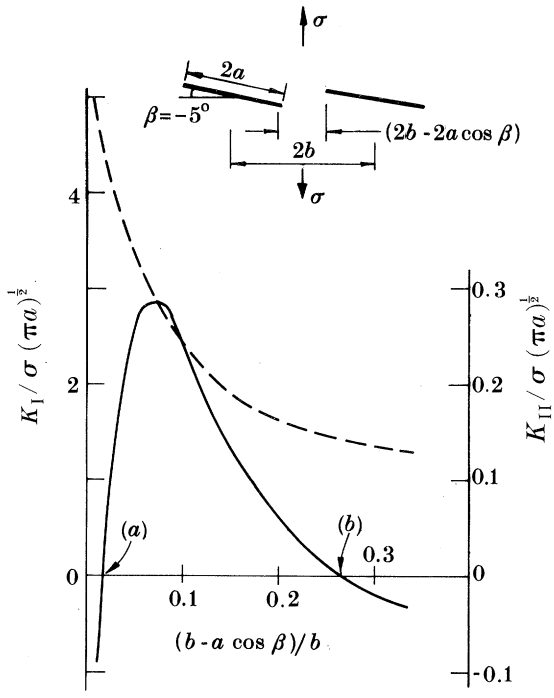

Figure 3. Effect of crack spacing upon stress intensity factors. When K_{II} is positive the cracks kink away from each other, and the cracks repel. When K_{II} is negative, the cracks attract each other. Crack angle $\beta = -5°$. (*a*) $a/b = 0.99$, (*b*) $a/b = 0.74$. ——, K_I; – – –, K_{II}.

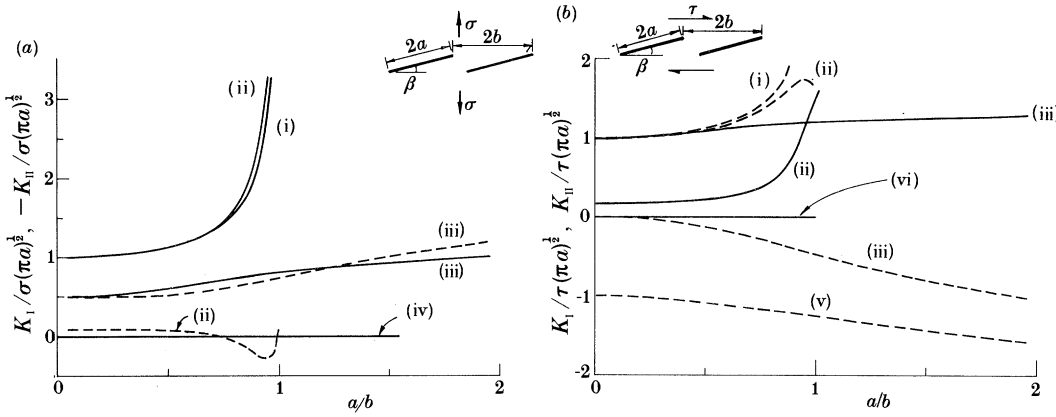

Figure 4. Stress intensity factors for an infinite array of straight cracks under (*a*) remote tension, and (*b*) remote shear. ——, K_I; – – –, K_{II}. (i) $\beta = 0°$; (ii) $\beta = -5°$; (iii) $\beta = -45°$; (iv) K_I, K_{II} for $\beta = -90°$, K_{II} for $\beta = 0°$; (v) $\beta = -90°$; (vi) K_I for $\beta = 0°$.

finding is observed for cracks very close together. However for a crack spacing in the range $0.74 < a/b < 0.99$, K_{II} is positive and the cracks repel each other. This is consistent with the common observation that cracks coalesce by one crack tip growing into the flank of another crack rather than by crack tip joining crack tip. Melin (1983) came to the same conclusion by use of a perturbation analysis.

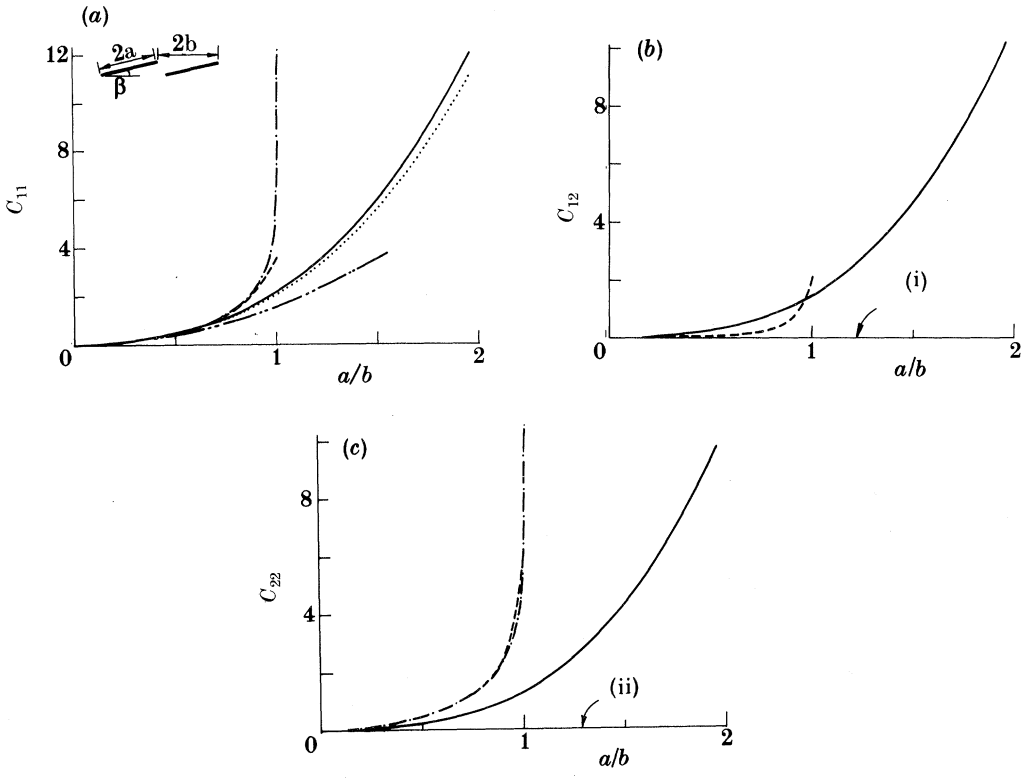

Figure 5. Extra compliance for an array of straight cracks. (*a*) C_{11}, (*b*) C_{12} and (*c*) C_{22} as a function of crack length and crack orientation. ——, $\beta = -45°$; – – –, $\beta = -5°$; —·—·, $\beta = 0°$; ·····, $\beta = -90°$; ——·——, isolated crack solution, $\beta = 0°$, $-90°$. (i) $\beta = 0°$, $-90°$; (ii) $\beta = -90°$.

4.2. *Effect of crack orientation and crack spacing on stress intensity factors and extra compliance*

The stress intensities and extra compliance for any array of straight cracks are given in figures 4 and 5 respectively, plotted as a function of crack length.

In all cases for a/b less than approximately 0.1, the cracks behave as isolated cracks and the stress intensity factors scale with the square root of crack length. For the special case $\beta = 0°$, analytic expressions have been found by Koiter (1959) for the stress intensities and the extra compliance

$$\left.\begin{aligned} \begin{bmatrix} K_{\mathrm{I}} \\ K_{\mathrm{II}} \end{bmatrix} &= (2b \tan(\pi a/2b))^{\frac{1}{2}} \begin{bmatrix} \sigma_y^{\infty} \\ \sigma_{xy}^{\infty} \end{bmatrix}, \\ C_{11} = C_{22} &= -(4/\pi) \ln(\cos(\pi a/2b)), \quad C_{12} = C_{21} = 0. \end{aligned}\right\} \tag{4.1}$$

The numerical results agree with these expressions, forming a check of the calculation. As a/b approaches unity $K_{\mathrm{I}}, K_{\mathrm{II}}$ and $C_{11} = C_{22}$ become unbounded, and the cracks coalesce.

Now consider the cracks rotated slightly so that $\beta = -5°$. The solutions for K_{I} due to σ_y^{∞} and K_{II} due to σ_{xy}^{∞} are similar to the corresponding solutions for $\beta = 0°$. Also, the extra compliance C_{ij} changes little as β is decreased from $\beta = 0°$ to $\beta = -5°$.

For the case of $\beta = -45°$ and remote tension σ_y^{∞}, the widely spaced cracks suffer equal normal and shear loading on axes aligned with the cracks. Over the whole

range of a/b considered, $0 < a/b < 2$, the stress intensities normalized by $a^{\frac{1}{2}}$ are essentially constant; in this sense the cracks do not interact strongly. The mode II stress intensity K_{II} is positive suggesting that the cracks will branch away from the neighbouring crack: the cracks repel each other.

Under remote shear, widely spaced cracks at $\beta = -45°$ suffer tensile loading normal to the crack with zero shear parallel to the crack. As a/b is increased the cracks interact slightly: $K_I/\tau(\pi a)^{\frac{1}{2}}$ increases from unity to 1.3 as a/b is increased from 0 to 2. The mode II stress intensity K_{II} is negative for $0 < a/b < 2$, suggesting that the cracks attract each other with subsequent crack growth.

The compliance coefficients C_{11} and C_{22} for $\beta = -45°$ are less than for $\beta = 0°$ for all a/b investigated, as we would expect. The orientation $\beta = -45°$ gives strong coupling between remote loading in one direction and the extra displacement in the other direction. Thus, C_{12} is of similar magnitude to C_{11} and C_{22}.

Last, consider cracks orientated at $\beta = -90°$. The presence of the cracks has no influence on the stress field under remote loading σ_y^∞. Under shear loading σ_{xy}^∞, K_{II} is finite and negative, and increases approximately as the square root of crack length. The only non-zero compliance component C_{11} is little different from the case $\beta = -45°$. The K solutions for $\beta = -90°$ and remote shear have been given previously by Benthem & Koiter (1973) and by Kamei & Yokobori (1974). Kamei & Yokobori (1974) used the dislocation distribution method and the results of the current study are in agreement to within the 1% stated accuracy of their results. For large a/b Benthem & Koiter find

$$K_{II} \sim -\tau(\pi a)^{\frac{1}{2}}(3/\pi)^{\frac{1}{2}}(a+0.2865b)/(ab)^{\frac{1}{2}} \tag{4.2a}$$

$$\sim -\tau(3a)^{\frac{1}{2}}(a/b)^{\frac{1}{2}} + O(b^{\frac{1}{2}}) \tag{4.2b}$$

The first term on the right-hand side of (4.2b) may be derived by considering the material between the cracks to behave as a beam under bending and shear. The stress intensity factor K_{II} is calculated by considering the energy released, $\mathcal{G} \cdot \delta a$, when each crack is advanced an increment δa and by using the well-known formula

$$(E/(1-\nu^2))\,\mathcal{G} = K_{II}^2, \tag{4.3}$$

where $\mathcal{G}$ is the energy release rate per crack tip. The extra compliance by this method is

$$C_{11} = (a/b)^3. \tag{4.4}$$

Comparison with numerical calculation shows that equations (4.2b) and (4.4) are accurate to within a few percent for b/a less than 0.1.

5. Evolution of crack array under shear

In this section, results are presented for the growth of a crack array under remote shear. The issue of crack stability for a cracked strip of finite height under prescribed remote displacement is addressed. Finally, the response of the crack array under shear is used to model the contribution to toughening of a macrocrack by microcrack bridging.

5.1. *Growth of a crack array under shear*

An incremental crack advance calculation was performed where an array of initially straight cracks of length $a_0/b = 0.1$ was grown under shear until the cracks coalesced at $a/b = 2.70$. We assumed that the cracks nucleated normal to the

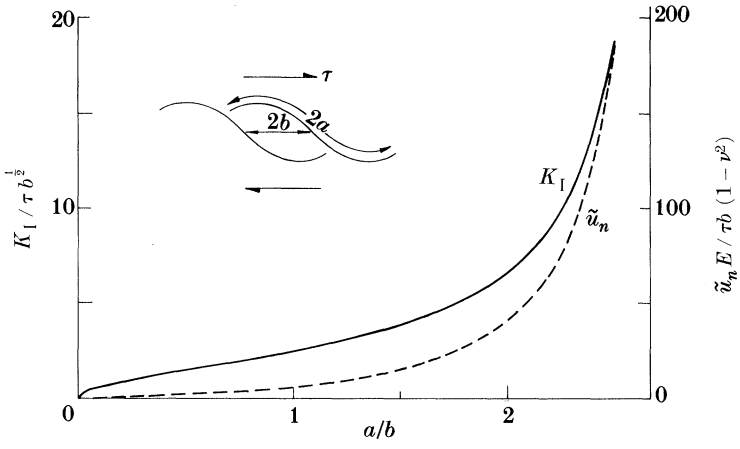

Figure 6. Evolution of mode I stress intensity K_I and normal crack opening at crack mid-point $\tilde{u}_n$, for an array of cracks under remote shear. Initial crack length $a_0/b = 0.1$, initial orientation $\beta = -45°$.

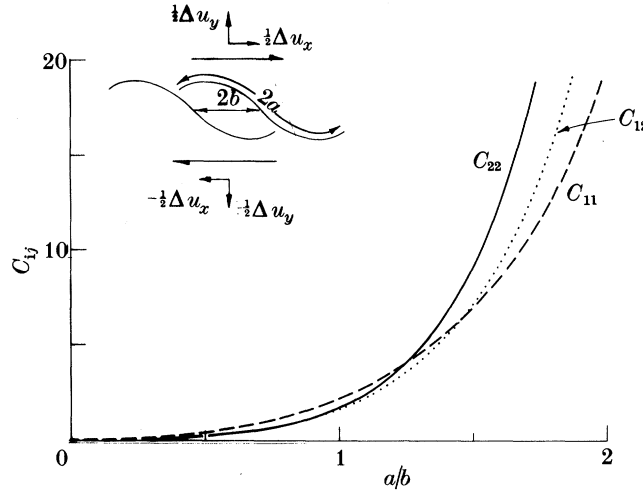

Figure 7. Extra compliance for an array of cracks which grow under remote shear.
$\Delta u_x E/2b(1-\nu^2) = C_{11}\sigma^\infty_{xy} + C_{12}\sigma^\infty_y$, $\Delta u_y E/2b(1-\nu^2) = C_{12}\sigma^\infty_{xy} + C_{22}\sigma^\infty_y$.

direction of principal tensile stress at $\beta = -45°$. The cracks were allowed to evolve to arbitrary shape of piecewise constant curvature in steps $\Delta a/b = 0.2$, such that K_{II} vanishes at the crack tip. Results are presented in figures 6 and 7.

The mode I stress intensity K_I and crack opening $\tilde{u}_n$ at crack mid-point increase dramatically with increasing crack length until the cracks coalesce (figure 6). As shown in the insert of figure 6 the curvature of the cracks is always positive, and the maximum height of any crack in the y-direction is 0.84 times the crack spacing $2b$.

The components of extra compliance are of similar magnitude and increase monotonically with crack extension (figure 7). Initially C_{11} is larger than the other components. At a/b greater than approximately 1.25, C_{22} becomes dominant.

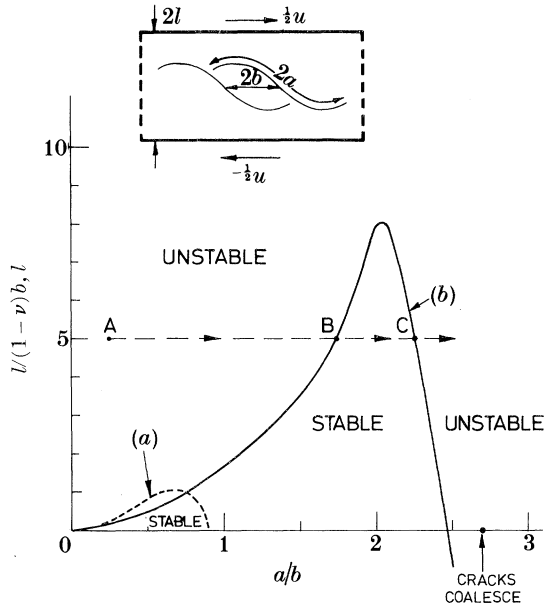

Figure 8. Stability of a crack array in a strip of height $2l$ under prescribed shear displacement, u. For comparison, the dotted line gives the boundary of stability for an array of straight collinear cracks under prescribed normal displacement. (*a*) l/b, collinear cracks under prescribed normal displacement, (*b*) $l/(1-\nu)b$, shear case.

5.2. *Stability of a cracked strip of finite height under remote shear*

Consider a crack array in a strip of finite height $2l$ and infinite length as shown in figure 8. The material is assumed to be perfectly brittle with the condition for crack advance $K_{\mathrm{I}} = K_{\mathrm{Ic}}$ and $K_{\mathrm{II}} = 0$, where K_{Ic} is the plane strain fracture toughness. Under prescribed loading at $y = \pm l$, the crack array is unstable in the sense that

$$[\mathrm{d}K_{\mathrm{I}}/\mathrm{d}a]_{\sigma_{ij}^{\infty}} > 0. \tag{5.1}$$

We shall show that there exists a finite strip height below which the crack array is stable under prescribed displacements at $y = \pm l$.

First, the compliance of the strip $\boldsymbol{C}^{\mathrm{s}}$ is decomposed into the compliance of the uncracked strip $\boldsymbol{C}^{0}$ and the extra compliance due to the presence of the crack array $\boldsymbol{C}^{e}$. To a very good approximation the extra compliance may be identified with the extra compliance for the crack array in an infinite solid, i.e. $\boldsymbol{C}^{e} = \boldsymbol{C}$. Thus,

$$\boldsymbol{C}^{\mathrm{s}}(a/b) = \boldsymbol{C}^{0} + \boldsymbol{C}(a/b). \tag{5.2}$$

For the case of a cracked finite strip under simple shear the average shear stress τ on the faces of the strip due to a prescribed relative displacement u between top and bottom faces is given by

$$u = (\tau/\mu)\,(2l + (2b(1-\nu^2)/E)\,\mu C_{11}(a/b)). \tag{5.3}$$

The two terms on the right-hand side of (5.3) represent the uncracked and extra compliances of the strip.

The stress intensity factor K_{I} at each crack tip in the crack array is given by

$$K_{\mathrm{I}} = \tau b^{\frac{1}{2}} f(a/b), \tag{5.4}$$

where the non-dimensional function $f(a/b)$ depends upon the particular crack geometry.

We shall first derive the stability condition and then apply it to the case of an array of curved cracks growing under remote shear. For stability under prescribed displacements we require

$$[\mathrm{d}K_{\mathrm{I}}/\mathrm{d}a]_u < 0. \tag{5.5}$$

Let each crack tip advance by δa under constant remote u. Then, equation (5.3) gives

$$\left[\frac{\mathrm{d}\tau}{\mathrm{d}a}\right]_u = -\tau\left(\frac{2b(1-\nu^2)\,\mu}{E}\frac{\partial C_{11}}{\partial a}\right)\left(2l+\frac{2b(1-\nu^2)\,\mu}{E}C_{11}\right)^{-1} \tag{5.6}$$

and equation (5.4) yields

$$[\mathrm{d}K_{\mathrm{I}}/\mathrm{d}a]_u = [\mathrm{d}\tau/\mathrm{d}a]_u\, b^{\frac{1}{2}} f(a/b) + (\tau/b^{\frac{1}{2}}) f'(a/b). \tag{5.7}$$

At the onset of instability the inequality in (5.5) is replaced by an equality sign, and (5.7) may be rewritten via (5.6) as

$$l/(1-\nu)\,b = \tfrac{1}{2}(f(a/b)/f'(a/b))\,C'_{11}(a/b) - \tfrac{1}{2}C_{11}(a/b) \tag{5.8}$$

The functions $f(a/b)$ and $C_{11}(a/b)$ for an array of curved cracks growing under remote shear tractions (or displacements) and $\sigma_y^\infty = 0$ are given in figures 6 and 7. The corresponding stability plot is constructed using (5.8) and is shown in figure 8. Consider a strip of height $l/(1-\nu)\,b = 5$, as shown in figure 8. After nucleation to an initial crack length given by points A on the figure, the cracks are unstable. They will advance dynamically until they attain a length comparable with that given by the stability boundary, point B. With further remote shear displacement of the strip boundaries, the cracks grow stably until point C is reached, and the crack array becomes unstable again. The cracks then coalesce. We only expect to observe cracks in the range B $\rightarrow$ C. Note that the cracks do not kink at the onset of instability since K_{II} equals zero at this instant; the compliance at the onset of instability depends only on the current geometry and not on the loading increment. It is clear from figure 8 that for $l/(1-\nu)\,b$ less than 8, the crack array is stable only at intermediate crack lengths.

Results for a collinear crack array in a strip of height $2l$ under remote tension are included in figure 8. An expression for the critical strip height at the stability limit follows directly from Koiter's analysis (1959)

$$l/b = (4/\pi)\ln(\cos(\pi a/2b)) + (8/\pi)\sin^2(\pi a/2b). \tag{5.9}$$

By comparison with the crack array under shear, the crack array under tension is unstable unless l/b is very small, that is less than unity. At such small l/b values the approximation $\boldsymbol{C}^e = \boldsymbol{C}$ may break down.

5.3. *Crack bridging due to an array of microcracks*

Advance of a microcrack through a brittle solid such as a polycrystalline ceramic or a polymer is often associated with microcracking ahead of the crack tip. Ortiz (1988) has calculated the remote strain energy release rate $\mathscr{G}_{\mathrm{Ia}}$ required to advance a tensile model I macrocrack with a microcrack zone at its tip. For microcracks which are small initially compared with their spacing, he finds that $\mathscr{G}_{\mathrm{Ia}}$ is little different from the toughness $\mathscr{G}_{\mathrm{Ic}}$ of the undamaged material. Ortiz shows that the decrease in $\mathscr{G}_{\mathrm{Ia}}$ due to pre-existing microcracks ahead of the main crack is of similar magnitude to the increase in $\mathscr{G}_{\mathrm{Ia}}$ associated with crack tip shielding by the microcracks.

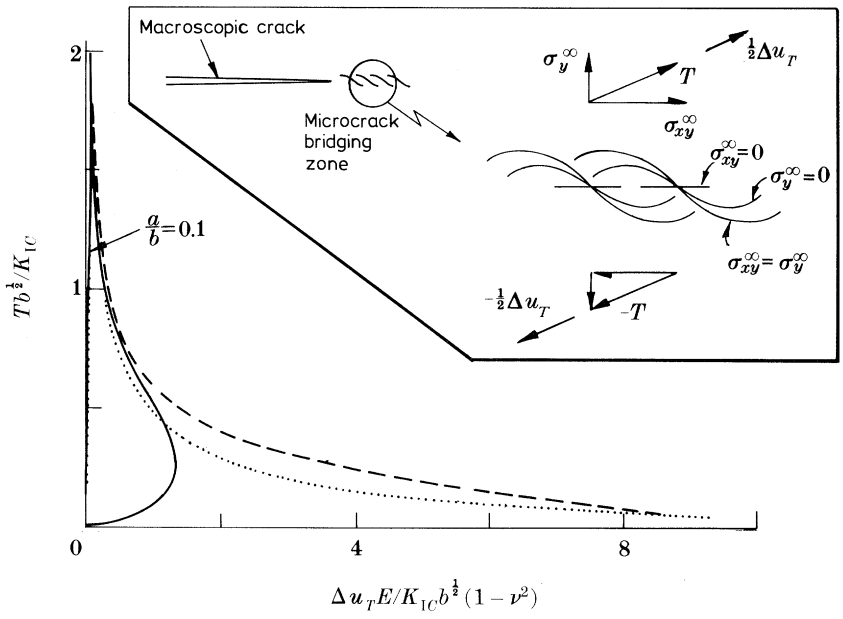

Figure 9. Remote traction versus extra displacement response of a crack array under remote proportional loading. This response provides the elastic spring stiffness for a microcrack zone at the tip of a macroscopic crack. ——, tension case ($\sigma_{xy}^\infty = \sigma_x^\infty = 0$); – – –, shear case ($\sigma_y^\infty = \sigma_x^\infty = 0$); ·····, equal tension and shear ($\sigma_x^\infty = 0$, $\sigma_{xy}^\infty = \sigma_y^\infty$).

Here we assume that the macroscopic crack grows by the advance and coalescence of microcracks ahead of the main crack tip, and we neglect shielding effects. It is envisaged that an array of microcracks of constant spacing $2b$ exists ahead of the main crack tip. Remote from the crack tip the microcracks are of vanishingly small initial length $a_0/b \ll 1$. But as the crack tip is approached the microcrack length increases, until coalescence occurs at the main crack tip. A straightforward energy argument gives the strain energy release rate $\mathscr{G}_{\mathrm{Ia}}$ required to advance the macroscopic crack by a unit distance in a self-similar direction

$$\mathscr{G}_{\mathrm{Ia}}/\mathscr{G}_{\mathrm{Ic}} = (a_f - a_0)/b \tag{5.10}$$

where a_0 is the initial microcrack length far from the main crack tip, and a_f is the microcrack length at coalescence. Henceforth, we shall assume $a_0 \ll a_f$ and may be neglected. Under remote tension the microcracks are collinear with the main crack, giving $a_f = b$ and $\mathscr{G}_{\mathrm{Ia}} = \mathscr{G}_{\mathrm{Ic}}$. For more general remote loading, we may still use equation (5.10) to estimate the remote energy release rate $\mathscr{G}_{\mathrm{Ia}}$ for coplanar growth of a macroscopic crack through a microcrack array. For example, under pure shear we find $\mathscr{G}_{\mathrm{Ia}}/\mathscr{G}_{\mathrm{Ic}} = a_f/b = 2.7$.

An alternative crack advance mechanism is by kinking from the tip of the main crack. For pure shear, the remote energy release rate for kinking $\mathscr{G}_{\mathrm{Ik}}$ is $\mathscr{G}_{\mathrm{Ik}}/\mathscr{G}_{\mathrm{Ic}} = 0.69$ (Bilby *et al.* 1977), and is energetically favourable. In practice, collinear mode II crack growth is observed (Fleck *et al.* 1990), Johnson & Mangalgiri (1987), and Evans & Hutchinson (1989)). The may be due to trapping of the main crack by neighbouring microcracks.

Further aspects of the propagation of a macrocrack through a microcrack array may be investigated using a cohesive zone model. In this approach, the remote

traction versus extra displacement response of an evolving array of microcracks provides the elastic spring constant in a crack bridging cohesive zone model. Ortiz (1988) has calculated the spring constant for mode I loading. Here, we consider arbitrary remote loading. Assuming the microcracks grow under the condition $K_{\mathrm{I}} = K_{\mathrm{Ic}}$ and $K_{\mathrm{II}} = 0$, the remote traction T against extra displacement Δu_T response may be calculated from (3.11) and (5.4). Here, $T = (\sigma_{xy}^{\infty 2} + \sigma_y^{\infty 2})^{\frac{1}{2}}$ is the magnitude of the remote traction on an infinite solid containing an array of microcracks and Δu_T is the extra displacement resolved in the direction of the remote traction. Results are given in figure 9 for several loading cases. In each case we assume that microcracks of zero initial length a_0 nucleate normal to the direction of remote principal tensile stress, and we take $\sigma_x^{\infty} = 0$. As discussed by Rice (1968), the J integral may be used to show that the area under the T against Δu_T curve equals the remote energy release rate $\mathscr{G}_{\mathrm{Ia}}$, and a direct evaluation gives (5.10) as before.

6. Evolution of a crack array under a range of stress states

The growth of an array of microcracks in an infinite solid was calculated for a wide range of remote loading specified by $\sigma_y^{\infty}/\sigma_{xy}^{\infty}$ and $\sigma_x^{\infty}/\sigma_{xy}^{\infty}$. In each case, cracks were nucleated at a small initial length $a/b = 0.1$, normal to the direction of maximum principal tensile stress. Typical cracking patterns are presented in figure 10. Note that the cracking pattern depends only on the stress state.

Three types of response were observed:

(*a*) no cracks nucleate when the maximum principal tensile stress is negative; the conditions for this are,

$$\sigma_x^{\infty}\,\sigma_y^{\infty}/(\sigma_{xy}^{\infty}\,\sigma_{xy}^{\infty}) > 1, \quad \text{with } \sigma_x^{\infty} < 0 \quad \text{and } \sigma_y^{\infty} < 0; \tag{6.1}$$

(*b*) cracks nucleate and coalesce; as the crack tip approaches the neighbouring crack K_{I} increases dramatically; and

(*c*) cracks nucleate and grow to a steady state angle and constant K_{I} value; no coalescence occurs.

Calculation of the crack opening profile and the K_{I} history shows that cracks which nucleate remain open along their length and K_{I} remains positive. Thus, issues of crack face interference or crack arrest do not arise.

Consider first the case of $\sigma_y^{\infty}/\sigma_{xy}^{\infty}$ fixed with $\sigma_x^{\infty} = 0$ (figure 10*a*). Cracks nucleate and coalesce for $\sigma_y^{\infty}/\sigma_{xy}^{\infty} > -0.4$. As $\sigma_y^{\infty}/\sigma_{xy}^{\infty}$ decreases from infinity to -0.4 the curvature of the cracks increases. This is reflected in a plot of crack length at coalescence a_f/b against $\sigma_y^{\infty}/\sigma_{xy}^{\infty}$ in figure 11*a*. As discussed in the previous section, the quantity a_f/b may be reinterpreted as the remote energy release rate for propagation of a macrocrack with an array of microcracks in the process zone at its tip. When $\sigma_y^{\infty}/\sigma_{xy}^{\infty}$ is less than -0.4 the array of cracks nucleate and grow to a steady state angle orientation β_f. Calculations show that this angle β_f is equal to that of the remote traction

$$\beta_f = \arctan(\sigma_y^{\infty}/\sigma_{xy}^{\infty}). \tag{6.2}$$

For other loadings with finite σ_x^{∞}, it is observed that (6.2) remains valid.

In steady state, the ligaments between the microcracks behave as slender beams under axial loadings and bending. A simple energy argument shows that K_{I} is finite and constant at each crack tip. Typical values for K_{I} from the full numerical solution are presented in figure 12; these values are for cracks which are essentially in steady state at $a/b \approx 5$. It was not possible to calculate the value of K_{I} in steady state using

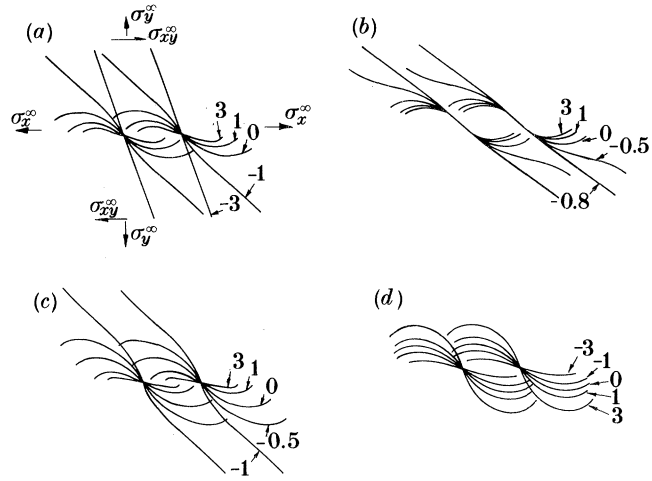

Figure 10. Evolution of an array of microcracks under a range of stress states. (*a*) $\sigma_x^\infty = 0$, (*b*) $\sigma_x^\infty = \sigma_y^\infty$, (*c*) $\sigma_x^\infty = -\sigma_y^\infty$, (*d*) $\sigma_y^\infty = 0$. In cases (*a*)–(*c*) the numbers refer to $\sigma_y^\infty/\sigma_{xy}^\infty$. In case (*d*) the numbers refer to $\sigma_x^\infty/\sigma_{xy}^\infty$.

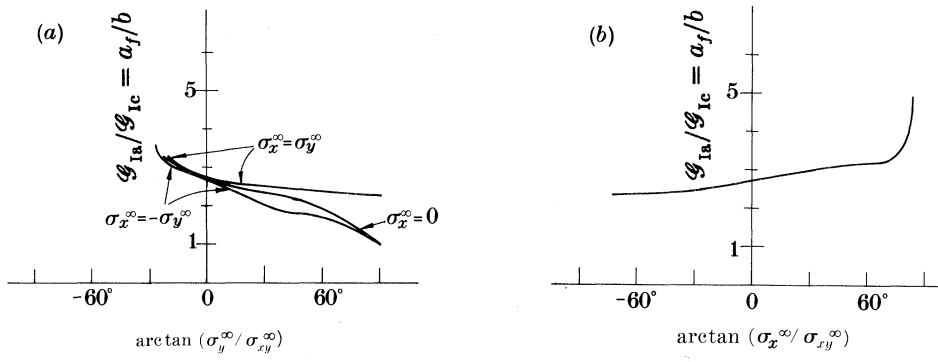

Figure 11. Apparent toughness of an array of microcracks which have evolved under remote proportional loading. The ratio of apparent toughness to mode I toughness $\mathcal{G}_{Ia}/\mathcal{G}_{Ic}$ is equal to the final crack length at coalescence divided by the crack spacing, a_f/b. (*a*) General case $\sigma_y^\infty \neq 0$, (*b*) $\sigma_y^\infty = 0$.

energy arguments as the bending moment in the ligament between cracks depends upon the details of the crack shape in the early stages of crack growth.

Now consider the loading $\sigma_x^\infty = \sigma_y^\infty$, with finite σ_{xy}^∞. Typical cracking patterns and a_f/b are given in figures 10*b* and 11*a* respectively. The remote stress state consists of hydrostatic loading with superimposed shear. For $\sigma_y^\infty/\sigma_{xy}^\infty < -1$, no tensile stresses exist and no cracks nucleate. At larger $\sigma_y^\infty/\sigma_{xy}^\infty$ cracks always nucleate at $\beta_0 = -45°$ (figure 10*b*). For $-1 < \sigma_y^\infty/\sigma_{xy}^\infty < -0.4$ cracks nucleate but do not coalesce; they evolve to a steady-state angle given by (6.2). The array of microcracks coalesce for $\sigma_y^\infty/\sigma_{xy}^\infty > -0.4$; with increasing $\sigma_y^\infty/\sigma_{xy}^\infty$ above this limit the curvature of the cracks increases and a_f/b decreases (see figures 10*b* and 11*b*). As $\sigma_y^\infty/\sigma_{xy}^\infty$ is increased to very large values $\sigma_y^\infty/\sigma_{xy}^\infty \gg 1$, the cracks remain at an initial orientation of $\beta_0 = -45°$. This feature causes a_f/b to be greater than unity as $\sigma_y^\infty/\sigma_{xy}^\infty$ tends to infinity, as shown in figure 11*a*.

The loading $\sigma_x^\infty = -\sigma_y^\infty$, with finite σ_{xy}^∞ has the property that the hydrostatic stress is zero. Typical cracking patterns are given in figure 10*c*. They are similar in

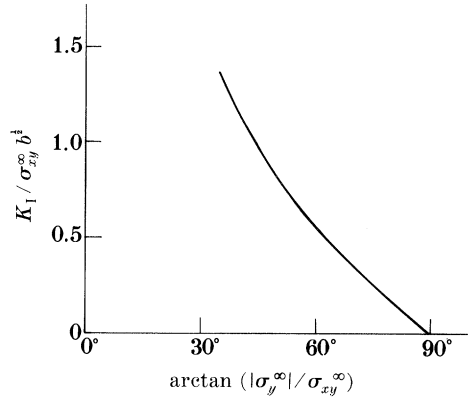

Figure 12. Stress intensity factor at tip of each microcrack, after the array of microcracks has evolved to a steady state orientation. The stress component σ_y^{∞} is negative. $\sigma_x^{\infty} = 0$.

qualitative terms to that due to the loading $\sigma_x^{\infty} = 0$. For $\sigma_y^{\infty}/\sigma_{xy}^{\infty} < -0.8$ cracks nucleate but do not coalesce. At larger $\sigma_y^{\infty}/\sigma_{xy}^{\infty}$, cracks nucleate and coalesce. In the limit of $\sigma_y^{\infty}/\sigma_{xy}^{\infty}$ tending to infinity, the cracks become collinear and a_f/b tends to unity (figure 11*b*).

For completeness, the effect of varying $\sigma_x^{\infty}/\sigma_{xy}^{\infty}$ with $\sigma_y^{\infty} = 0$ upon the cracking pattern is given in figure 10*d* and in figure 11*b*. For all finite $\sigma_x^{\infty}/\sigma_{xy}^{\infty}$ cracks nucleate and coalesce. As $\sigma_x^{\infty}/\sigma_{xy}^{\infty}$ is increased from negative infinity to positive infinity, β_0 decreases from 0 to $-90°$ and a_f/b increases from unity to infinity (figure 11*b*). In the limit of a finite σ_x^{∞}, $\sigma_{xy}^{\infty} = \sigma_y^{\infty} = 0$, the cracking pattern consist of a line of vertical cracks which do not coalesce. The stress intensity factor K_I for this limiting case has been calculated by Fichter (1967), and by Benthem & Koiter (1973), amongst others. A summary of the solution is given by Tada *et al.* (1985). In the limit $a/b \to \infty$, K_I is given by

$$K_I = \sigma_x^{\infty} b^{\frac{1}{2}}. \tag{6.3}$$

7. Fracture map and case studies

A fracture map is constructed, showing how the cracking pattern of a crack array depends upon remote stress state. We take an axes arctan $(\sigma_x^{\infty}/\sigma_{xy}^{\infty})$ and arctan $(\sigma_y^{\infty}/\sigma_{xy}^{\infty})$ (see figure 13). Then, all possible stress states are contained within a square of extent $\pm 90°$ in both directions. The origin corresponds to a stress state of pure shear, while the axes and diagonals of the map constitute the four types of stress state summarized in figures 10 and 11.

The map summarizes the three types of cracking response:

(A) no nucleation (the criterion for no nucleation (equation (6.1)) prescribes a region in the map with straight boundaries, as shown in figure 13);

(*B*) nucleation and coalescence; and

(*C*) nucleation but no coalescence.

The boundary between regions (B) and (C) is found by iteration. Data points are included in figure 13 to show the precision by which the boundary has been determined; typically, the error in location is less than 5% in either coordinate.

Region B, consisting of nucleation and coalescence, dominates the map. It appears that for $\sigma_y^{\infty}/\sigma_{xy}^{\infty} \gtrsim -0.6$ cracks nucleate and coalesce, with $\sigma_x^{\infty}/\sigma_{xy}^{\infty}$ exerting only a secondary influence. Contours of constant a_f/b have been added to region (B). These

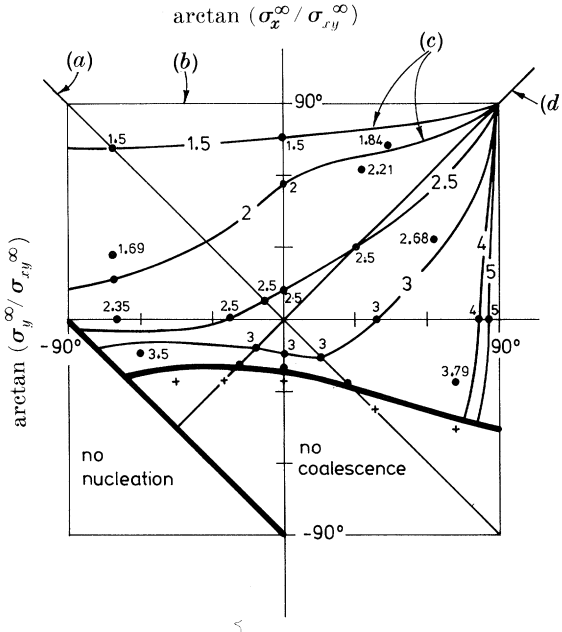

Figure 13. Development of fracture map for an array of microcracks. Three regimes exist: no nucleation, no coalescence and coalescence. Individual data points marked ● are used to construct contours of constant a_f/b in the coalescence régime, + in the no coalescence régime. (*a*) $\sigma_x^\infty = -\sigma_y^\infty$, (*b*) $a_f/b = 1$, (*c*) contours of a_f/b, (*d*) $\sigma_x^\infty = \sigma_y^\infty$.

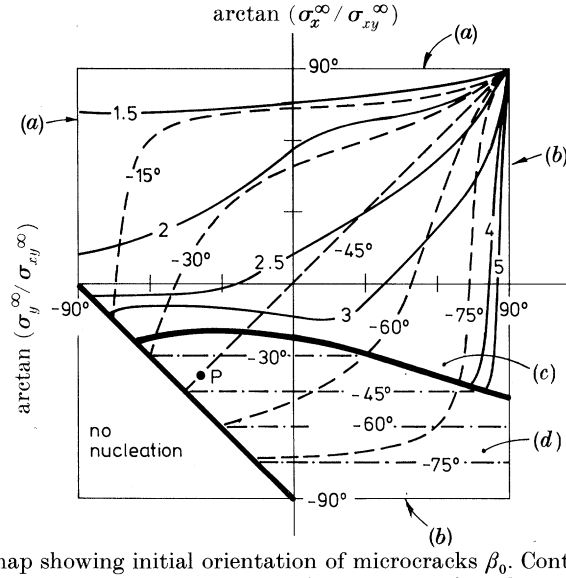

Figure 14. Fracture map showing initial orientation of microcracks β_0. Contours of a_f/b are given in the coalescence regime, and contours of final crack orientation β_f in the regime of no coalescence. Point P refers to the stress state which is predicted to exist during the formation of the echelon cracks in carboniferous graywacke in figure 15*b*. ——, a_f/b; – – –, β_0; ·–·–·, β_f. (*a*) $\beta_0 = 0°$; (*b*) $\beta_0 = -90°$; (*c*) coalescence; (*d*) no coalescence.

contours have been constructed from the values of a_f/b given in figure 11 and from a number of additional loading cases. Individual data points used in the construction of the contours are included in figure 13.

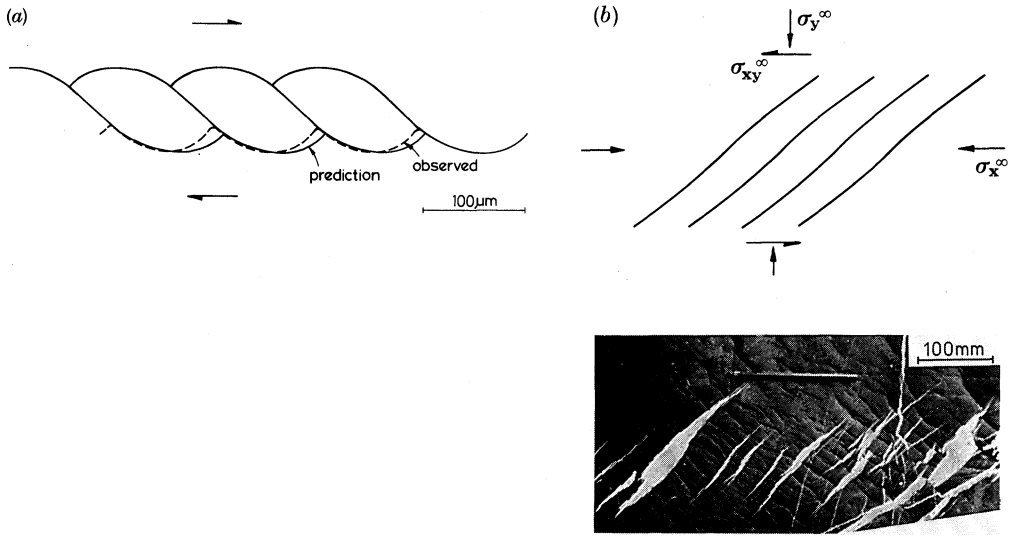

Figure 15. (*a*) Comparison of predicted and observed crack path in PMMA under simple shear. $\dot{\gamma} = 10^{-3}\ \mathrm{s}^{-1}$, T = 20 °C. (*b*) Comparison of predicted and observed crack shape in carboniferous graywacke. The inferred stress state is given by point P in figure 14. The rock sample exists near Bude, Devon, England, and the photograph is reproduced with permission from Ramsay (1967).

When $\sigma_y^\infty/\sigma_{xy}^\infty$ is sufficiently large and negative, cracks nucleate but do not coalesce, region (C) of figure 13. It is observed that the cracks evolve to an orientation β_f given by equation (6.2).

Finally, we add contours of constant crack nucleation angle β_0 to the map. A Mohr's circle construction gives β_0 as

$$\cot 2\beta_0 = -\frac{1}{2}\left(\frac{\sigma_y^\infty}{\sigma_{xy}^\infty} - \frac{\sigma_x^\infty}{\sigma_{xy}^\infty}\right). \tag{7.1}$$

The resulting map, with individual data point removed, is given in figure 14. It is useful in fractographic analysis for calculating the remote stress state corresponding to an observed cracking pattern. Two such case studies are given, one for the failure of polymethyl methacrylate under simple shear and the other for shear banding in a carboniferous rock.

7.1. *Shear failure of polymethyl methacrylate*

Brittle failure in shear due to an array of tensile microcracks has been observed in polycarbonate and in polymethyl methacrylate (Fleck & Wright 1989; Fleck *et al.* 1990). Tests were performed on tubes in torsion. The stress state for shear loading lies at the origin of figure 14. A typical fracture surface profile for polymethyl methacrylate is compared with the predicted crack profile due to remote shear in figure 15*a*. Agreement between the predicted profile and observed profile is good.

7.2. *Shear localization in carboniferous graywacke*

Figure 15*b* shows a zone of quartz-filled tensile microcracks in carboniferous graywacke, reported by Ramsay (1967). The measured values of initial crack angle and final crack angle are $\beta_0 = -45°$ and $\beta_f = -39°$ respectively. This corresponds to

a remote stress state of $\sigma_y^\infty/\sigma_{xy}^\infty = -0.81$, $\sigma_x^\infty/\sigma_{xy}^\infty = -0.81$ and is marked by a point P in figure 14. The predicted crack shape for $\sigma_y^\infty/\sigma_{xy}^\infty = -0.80$, $\sigma_x^\infty/\sigma_{xy}^\infty = -0.80$ is included in figure 3.2*b* for comparison; the agreement in shape is excellent.

8. Concluding discussion

In this paper, we have examined the conditions required for brittle fracture in a localized shear band. In order for complete separation of material on either side of a shear band containing microcracks, the stress ratio $\sigma_y^\infty/\sigma_{xy}^\infty$ must exceed approximately -0.6 as shown in figure 14.

The main underlying assumptions of the analysis are the following.

1. Microcracks nucleate under tensile stress in a direction normal to the remote principal tensile stress. This appears to be a reasonable assumption for brittle solids such as ceramics and polymers, and for metallic solids under fatigue loading. Crazes in polymers also obey this criterion, as discussed by Ward (1983).

2. Under remote shear loading microcracks nucleate at constant spacing, in a row aligned with the direction of remote shear. This has experimental support but requires a theoretical justification; the mechanism by which a few existing microcracks trigger the formation of other microcracks in a collinear array is not understood.

3. The microcracks grow such that K_{II} vanishes at the crack tip. This growth criterion is reasonable for a perfectly brittle isotropic solid. It may require modification for anisotropic solids where internal structure dictates crack path.

4. Each microcrack grows at the same rate. This is not expected for a perfectly brittle solid, where a microcrack slightly longer than the others would grow fastest. Similar growth by all microcracks is expected when the matrix material displays an R-curve, such that crack growth resistance increases with crack advance.

The phenomenon of tensile microcracking in a shear band may be thought of as a nucleation induced localization. Once microcracks have nucleated, deformation is localized in the cracked band and the remote material unloads. In this sense, the phenomenon is similar to nucleation induced localization in high strength steels, which has been analysed by Hutchinson and Tvergaard (1987), and by Fleck *et al.* (1989).

The author thanks Professor J. W. Hutchinson for many helpful discussions, and Professor S. Maaløe for providing the reference on shear fracture of rocks. The author is grateful for part funding by a NATO Collaborative Research Grant fellowship during his visits to the Division of Applied Sciences, Harvard University, and for part support by the National Science Foundation under Grant MSM-88-12779.

Appendix. Calculation of the extra compliance

Introduction of a crack array into an infinite elastic solid under remote loading σ_{ij}^∞ leads to an additional displacement at infinity. We define the extra displacement Δu_i as the relative displacement between remote material above and below the crack array, due to the presence of the cracks. The extra compliance C_{ij} relates u_i and σ_{ij}^∞, see equation (3.12). We may calculate u_i and C_{ij} by the reciprocal theorem, as follows.

Consider two different loadings on the cracked body, as shown in figure 16. Loading

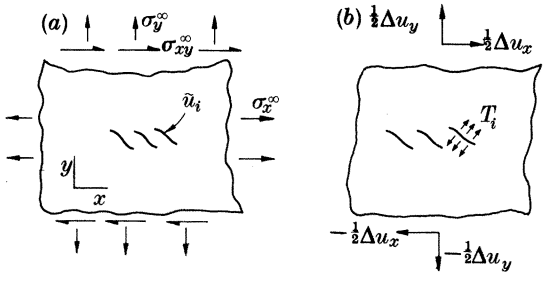

Figure 16. Use of reciprocity to determine the extra displacement Δu_i and the extra compliance C_{ij} due to an array of microcracks. (*a*) Loading A, (*b*) loading B.

A is the remote homogeneous loading σ_{ij}^∞, with zero traction on the cracks. Loading B consists of a traction $T_j = n_i \sigma_{ij}^\infty$ on the cracks (with the unit normal $\boldsymbol{n}$ pointing into the solid), and zero loading at infinity. This loading produces Δu_i at infinity. Loading B is the same as for the dislocation problem described in the body of the paper.

Define the crack opening displacement in problem A by $\tilde{u}_i$. Then the reciprocal theorem gives

$$2b(\sigma_y^\infty \Delta u_y + \sigma_{xy}^\infty \Delta u_x) = \int_{-a}^{a} T_x \tilde{u}_x + T_y \tilde{u}_y \, \mathrm{d}\xi$$

$$= \int_{-a}^{a} n_y \sigma_{xy}^\infty \tilde{u}_x + (n_x \sigma_{xy}^\infty + n_y \sigma_y^\infty) \tilde{u}_y \, \mathrm{d}\xi. \qquad \text{(A 1)}$$

References

Anderson, P. M., Fleck, N. A. & Johnson, K. L. 1990 Localization in shear due to cracking. *J. Mech. Phys. Solids.* **38**, 681–699.

Benthem, J. P. & Koiter, W. T. 1973 Asymptotic approximations to crack problems. In *Methods of analysis and solutions of crack problems* (ed. G. C. Sih), pp. 131–178. London: Noordhoff.

Bilby, B., Cardew, G. E. & Howard, I. C. 1977 Stress intensities at the tip of kinked and forked cracks. In *Fracture*, vol. 3, pp. 197–200. University of Waterloo Press.

Erdogan, F. & Gupta, G. D. 1972 On the numerical solution of singular integral equations. *Q. appl. Math.* **30**, 525–534.

Erdogan, F. & Sih, G. C. 1963 On the crack extension in plates under plane loading and transverse shear. *J. Basic Engng* **85**, 519–527.

Evans, A. G. 1985 Engineering property requirements for high performance ceramics. *Mater. Sci. Engng* **71**, 3–21.

Evans, A. G. & Hutchinson, J. W. 1989 Effects of non-planarity on the mixed mode fracture resistance of bimaterial interfaces. *Acta metall.* **37**, 909–916.

Fichter, W. B. 1967 Stresses at the tip of a longitudinal crack in a plate strip. *NASA Tech. Rep. TR-R-265*. NASA Langley.

Fleck, N. A. 1988 Creep fracture under remote shear. In *Proc. Euromech 239 on Mechanics of Creep Brittle Materials*, (ed. A. C. F. Cocks & A. R. S. Ponter). London: Elsevier.

Fleck, N. A., Hutchinson, J. W. & Tvergaard, V. 1989 Softening by void nucleation and growth in tension and shear. *J. Mech. Phys. Solids* **37**, 515–540.

Fleck, N. A., Stronge, W. J. & Liu, J. H. 1990 High strain rate response of polycarbonate and polymethyl methacrylate. *Proc. R. Soc. Lond.* A **429**, 459–479.

Fleck, N. A. & Wright, S. C. 1989 Deformation and fracture of polycarbonate at high strain rate. In *Proc. Fourth Int. Conf. on the Mechanical Properties of Materials at High Rates of Strain*, (ed. J. Harding).

Hutchinson, J. W. & Tvergaard, V. 1989 Softening due to void nucleation in metals. Fracture mechanics perspectives and directions. *ASTM STP 1020*, 61–83.

Johnson, W. S. & Mangalgiri, P. D. 1987 Influence of the resin on mixed mode interlaminar fracture, toughened composites. *ASTM STP 937*, 295–315.

Kamei, A. & Yokobori, T. 1974 Some results on stress intensity factors of the cracks and/or slip bands system. *Rep. Res. Inst. for Strength and Fracture of Materials* (*special issue*). Tohoku University, Sendai, Japan, **10** (2).

Koiter, W. T. 1959 An infinite row of collinear cracks in an infinite elastic sheet. *Ingen. Arch.* **28**, 168.

Melin, S. 1983 Why do cracks avoid each other? *Int. J. Fracture* **23**, 37–45.

Ortiz, M. 1988 Microcrack coalescence and macroscopic crack growth initiation in brittle solids, *Int. J. Solids Structures* **24**, 231–250.

Pollard, D. D., Segall, P. & Delaney, P. T. 1982 Formation and interpretation of dilatant echelon cracks. *Geol. Soc. Am. Bull.* **93**, 1291–1303.

Purslow, D. 1981 Some fundamental aspects of composites fractography. *Composites* **12**, 241–247.

Ramsay, J. G. 1967 Folding and fracturing or rocks. New York: McGraw-Hill.

Rice, J. R. 1968 Mathematical analysis in the mechanics of fracture. In *Fracture* (ed. H. Leibowitz), vol. 2, ch. 3, pp. 191–311. Academic Press.

Tada, H., Paris, P. C. & Irwin, G. R. 1985 The stress analysis of cracks handbook, 2nd edn. St. Louis, Missouri: Paris Productions, and Del Research Corporation.

Ward, I. M. 1983 Mechanical properties of solid polymers, 2nd edn. J. Wiley.

Yamamoto, H. 1978 Conditions for shear localization in the ductile fracture of void-containing materials. *Int. J. Fracture* **14**, 347–365.

Received 5 March 1990; accepted 23 May 1990